

Mechanism of Nanoparticle Formation in Self-Assembled Colloidal Templates: Population Balance Model and Monte Carlo Simulation

M. Ethayaraja, Kanchan Dutta, and Rajdip Bandyopadhyaya*

Department of Chemical Engineering, Indian Institute of Technology Kanpur, Kanpur 208016, India

Received: April 17, 2006; In Final Form: June 12, 2006

Modeling the nanoparticle formation mechanism in water-in-oil microemulsion, a self-assembled colloidal template, has been addressed in this paper by two formalisms: the deterministic population balance equation (PBE) model and stochastic Monte Carlo (MC) simulation. These are based on time-scale analysis of elementary events consisting of reactant mass transport, solid solubilization, reaction, coalescence-exchange of drops, and finally nucleation and growth of nanoparticles. For the first time in such a PBE model, realistic binomial redistribution of molecules in the daughter drops (after coalescence-exchange of two drops) has been explicitly implemented. This has resulted in a very general model, applicable to processes with arbitrary relative rates of coalescence-exchange and nucleation. Both the deterministic and stochastic routes could account for the inherent randomness in the elementary events and successfully explained temporal evolution of mean and variance of nanoparticle size distribution. This has been illustrated by comparison with different yet broadly similar experiments, operating either under coalescence (lime carbonation to make CaCO_3 nanoparticles) or nucleation (hydride hydrolysis to make $\text{Ca}(\text{OH})_2$ nanoparticles) dominant regimes. Our calculations are robust in being able to predict for very diverse process operation times: up to 26 min and 5 h for carbonation and hydrolysis experiments, respectively. Model predictions show that an increase in the external reactant addition rate to microemulsion solution is beneficial under certain general conditions, increasing the nanoparticle production rate significantly without any undesirable and perceptible change in particle size.

1. Introduction

Surfactant-based self-assemblies have a very well-defined shape and a tunable size in the range of nanometers. Spherical and cylindrical water-in-oil (w/o) and oil-in-water microemulsions (o/w), lamellar bilayers, vesicles, bicontinuous cubic, and birefringent phases are some examples of surfactant self-assemblies¹ obtained at various compositions of oil, water, and surfactant. These have been used as liquid-phase templates for the synthesis of nanoparticles of controlled size and shape.^{2–4} Production of inorganic nanoparticles, in particular, metals, metal oxides, semiconductors, and so forth, have assumed unparalleled importance in various current technologies; chiefly due to size- and shape-dependent novel magnetic, electronic, and optical properties compared to their bulk counterparts.^{5,6} In addition, the high surface area-to-volume ratio of particles leading to a large fraction of atoms being present on the nanoparticle surface enable them for applications in heterogeneous catalysis,⁷ lubricating oil additives,⁸ electronic and optical display devices,⁹ and so forth.

Among various self-assembled templates, w/o microemulsions are most widely employed for the preparation of water-insoluble nanoparticles. Microemulsions consist of nanosized, monodisperse water droplets dispersed in a continuous oil phase, with the drops having an adsorbed surfactant monolayer.¹⁰ In the rest of this paper, we use the term *drop* to denote a spherical water drop in a w/o microemulsion system. The size of a water drop can be tuned easily; it increases linearly with the molar ratio of water to surfactant used in the preparation.¹¹

For nanoparticle synthesis employing a w/o microemulsion solution (Figure 1), one of the reactants, A, in the form of a

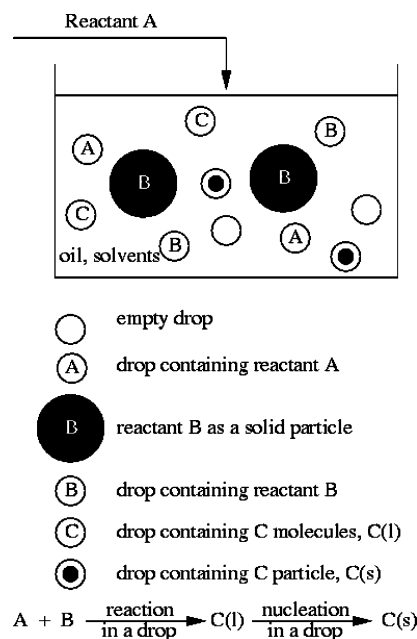


Figure 1. Schematic of the nanoparticle synthesis process. For brevity, water-in-oil microemulsion drops are shown without surfactants. Carbonation of lime: A, B, and C denote CO_2 , $\text{Ca}(\text{OH})_2$, and CaCO_3 , respectively. Hydrolysis of hydride: A, B, and C denote H_2O , CaH_2 , and $\text{Ca}(\text{OH})_2$, respectively.

gas or aqueous solution is added continuously to the microemulsion solution, whereby A gets transported into the drops (Figure 2a). Another reactant, B, is presolubilized in the drops by using its aqueous solution. In some cases, instead of or in addition to presolubilization, the reactant may be dispersed in the oil medium as micrometer-sized solid particles (Figure 1). In such a scenario, the drops solubilize the reactant while

* To whom correspondence should be addressed. E-mail: rajdip@iitk.ac.in. Phone: 91-512-259-7697. Fax: 91-512-259-0104.

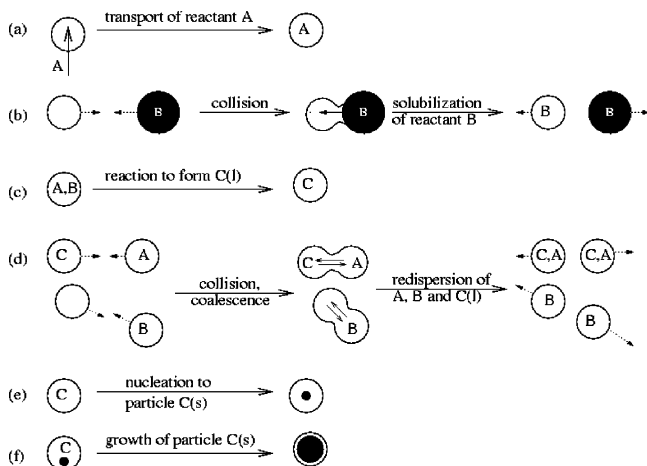


Figure 2. Various elementary steps in nanoparticle formation.

colliding with the dispersed particle (Figure 2b). In all cases, the reaction between A and B inside the drops (Figure 2c) causes the water-insoluble reaction product [C(l)] to attain supersaturation. The drops also undergo Brownian collision, thereby coalescing with other drops in the medium. In the process their contents are exchanged, followed by redispersion back into two equal-sized daughter drops (Figure 2d). A supersaturated drop can nucleate to form a solid particle [C(s)] (Figure 2e). The particle grows by exhausting supersaturation inside the drop, that is, by addition of C(l) molecules present in the latter (Figure 2f). The particle in a given drop can also grow by consuming C(l) of another drop during their pairwise Brownian collision and coalescence.

Experiments following the aforementioned routes or its variations using w/o microemulsion have been performed to make nanoparticles for use as lubricating oil additives. Kandori et al.,¹² for example, produced nanosized CaCO_3 particles by sparging CO_2 gas into a w/o microemulsion solution having presolubilized $\text{Ca}(\text{OH})_2$ in the drops. Roman et al.¹³ in addition, used micrometer-sized $\text{Ca}(\text{OH})_2$ solid particles dispersed in oil, which solubilized in the drops and reacted with CO_2 . We refer to the latter experiment as *carbonation of lime*. Delfort and co-workers did a series of experiments to prepare nanoparticles of $\text{Ca}(\text{OH})_2$ ¹⁴ (referred to as *hydrolysis of hydride*), sodium and potassium polyphosphates,¹⁵ and calcium thiophosphates¹⁶ in broadly similar methods, employing different combinations of dispersed solid particles and externally added reactants.

In contrast to reactive precipitation to make inorganic nanoparticles, as above, others have synthesized nanoparticles of organic compounds, which does not involve any reaction.^{17,18} A water-insoluble organic compound (e.g., nimesulide dissolved in a solvent like acetone, ethanol, etc.) is added to the continuous organic phase of a w/o microemulsion solution. Consequently, as acetone partitions between oil and water, it also brings nimesulide into the drops. The latter being insoluble in water, precipitates to form nanoparticles within the microemulsion drops. Further growth of the nanoparticles mediated by coalescence-exchange takes place as usual.

In contrast to these routes employing a single microemulsion solution, another popular method involves mixing two microemulsion solutions each containing different presolubilized reactants,¹⁹ leading to coalescence-exchange, reaction, nucleation, and growth of nanoparticles.

A complex interplay of various elementary steps occurring simultaneously (Figure 2) in these experiments gives rise to only partial understanding of the mechanism of nanoparticle formation. This is due to the nonuniform distribution of the number

of reactant and product molecules in drops, which are small and discrete in number, and in addition vary with time and influence the kinetics of these steps. Furthermore, the dynamics of the drops are strongly coupled because of continuous exchange of their contents by Brownian collision and coalescence. Another crucial fact is the inherent randomness associated with some of the elementary steps. Transport of reactant from the oil phase to a particular drop, coalescence-exchange of drops and reactant particles, and nucleation in a drop among a population of supersaturated drops are examples of this kind, where it is not known with certainty which particular drop or a pair of drops will undergo any of the above processes. It is therefore a challenge to understand the influence of various operational and control variables (for example, drop size, reactant concentration, reactant addition rate, etc.) on nanoparticle size distribution and thereby manipulate these for synthesizing material with desired characteristics.

Population balance equation (PBE)-based models^{20,21} are most appropriate for understanding particulate processes like nanoparticle formation. Few rate-based models,^{22,23} which are limited in scope and applicable to very specific systems were the first attempts to explain particle formation in w/o microemulsions. Subsequently, PBE models were developed by Natarajan et al.²⁴ and Bandyopadhyaya et al.^{25,26} The latter took into account the variation of the individual nucleation rate in each drop by considering the statistical distribution of molecules [C(l)] over the drops. However, their model is applicable only when coalescence-exchange of drops is faster than nucleation. In contrast, the coalescence-exchange rate can also be slower than or comparable to the nucleation rate. The relative rates of these two depend on various experimental factors. For example, the nature and type of surfactant and presence of cosurfactant can lead to variation in the flexibility of the interfacial surfactant layer and therefore alter the coalescence-exchange rate of drops. However, changes in the rate of reaction and solubility product of C(l) controls supersaturation and influences nucleation rate. So to understand the mechanism of nanoparticle formation in w/o microemulsion or for any self-assembled system, a general model applicable in all regimes of relative rates of the elementary steps is required. Other PBE based models have been proposed for nanoparticle formation in a homogeneous bulk aqueous medium; for example, growth of silica nanoparticles by reversible addition of monomers via the sol-gel mechanism²⁷ and aggregative growth of silver nanoparticles due to particle-particle interaction.²⁸ Although useful, models for particle formation in bulk medium cannot address the issues of partitioning, confinement, and exchange effects necessary to understand the role of self-assembled systems of concern to this paper.

Stochastic simulation techniques such as Monte Carlo (MC) simulation have also appeared in literature in conjunction with deterministic PBE models. The process of CdS nanoparticle formation employing two w/o microemulsion solutions was simulated by Bandyopadhyaya et al.,²⁹ using the concept of interval of quiescence.³⁰ Suitable modification and extension of their MC simulation scheme have been reported by other research groups.³¹⁻³⁴ However, these simulations do not account for reactant solubilization (Figure 2b) and transport of a reactant from the external oil phase (Figure 2a). This necessitates some changes in the MC scheme²⁹ to include these two steps, relevant to lime carbonation and hydride hydrolysis experiments of relevance here.

With this motivation, the time scales associated with each elementary step in the nanoparticle synthesis process are estimated in Section 2. PBE model and MC simulation based

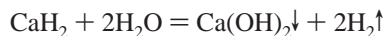
on the conclusions of time-scale analysis are presented in Sections 3 and 4, respectively. The results of the model and simulation are compared with experiments and discussed in Section 5 with final conclusions.

2. Time-Scale Analysis

Estimation of time scales of various elementary events depends on the experimental conditions. We therefore briefly discuss the two experiments: hydrolysis of hydride and carbonation of lime. Both are represented under a common thematic scheme in Figure 1, also showing important differences between them.

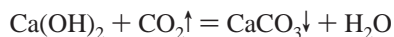
2.1. Hydrolysis of Hydride.¹⁴ A mixture consisting of C-24 calcium alkyl aryl sulfonate surfactant (90.4 g; average molecular weight 700), mineral oil (70.3 g), toluene (350 mL), and methanol (15 mL) was prepared. Calcium hydride particles (60 g) of micrometer size were dispersed in this mixture. A liquid mixture of tetrahydrofuran (155 mL) and water (44.9 g) at 5°C was added under stirring to the above for 5 h, giving nanoparticles in w/o microemulsion. Tetrahydrofuran (THF) partitions between the continuous oil phase and its interface with the drop, thus acting as a cosurfactant.³⁵ Water added diffuses into the drops and hydrolyses CaH₂, the latter being solubilized during drop-CaH₂ particle collisions.

The overall reaction is



Ca(OH)₂ is sparingly soluble in water and hence nucleates and grows as a solid particle inside the drop. From transmission electron microscopy (TEM) and small-angle X-ray scattering (SAXS), the particles were found to be disk-shaped.¹⁴ The final average particle size was of 20 nm diameter and 3 nm thickness.

2.2. Carbonation of Lime.¹³ A solution of xylene (150 mL) and mineral oil (22.5 g) served as the continuous oil medium, to which were added dialkyl aryl sulfonic acid (30.8 g; molecular weight 500), calcium hydroxide particles (26 g), and methanol (13 mL). Dialkyl aryl sulfonate surfactant was formed in situ by the reaction between Ca(OH)₂ and sulfonic acid. Water generated from this reaction was encapsulated by the surfactant, thus forming water drops in oil. Methanol partitioned between the drop core and the oil–water interface, acting as a cosurfactant. CO₂ gas was then sparged for 26 min to this w/o microemulsion solution. Reported data has been used to calculate and conclude that initially there were about 25 Ca(OH)₂ molecules in each drop.²⁶ Ca(OH)₂ was further solubilized throughout the process during collision of drops with Ca(OH)₂ particles. The sparged CO₂ diffused into the drops followed by reaction with solubilized Ca(OH)₂ as follows:



The insoluble reaction product, CaCO₃, nucleates and grows inside a drop. The average CaCO₃ particle diameter and coefficient of variation (CV) of particle size were reported as a function of time based on TEM and SAXS measurements.¹³

2.3. Time-Scale Calculations. If k_i is the rate constant of the i th elementary process (Figure 2), then its time scale is given by $\tau_i = 1/k_i$. On the basis of comparative time scales, rate-controlling events are identified and we propose a nanoparticle formation mechanism.

2.3.1. Transport of Gas/Liquid Reactant A (k_m) (Figure 2a). The rate of transport of a reactant molecule into a drop via the oil medium is given by

$$k_m = \frac{\alpha Q N_A}{N_{\text{drop}} M_w} \quad (1)$$

where α is the fraction of reactant A transported to the drops, Q is the mass flow rate of reactant, and N_{drop} is the total number density of drops. In the hydrolysis of hydride, THF retains some water in the oil and hence only a fraction (α) of the total amount of water added was available for reaction.³⁵

2.3.2. Solubilization of Reactant Particle B (k_{cp}) (Figure 2b). Quantitative models for solubilization of dispersed inorganic solid particles by drops of a w/o microemulsion solution have not been reported in literature. Therefore, we calculate the solubilization rate using the Brownian collision frequency of solid reactant B particle with the drops. This is given by the Smoluchowski³⁶ equation

$$q_p = \frac{2k_B T}{3\mu} \left[2 + \left(\frac{v_p}{v} \right)^{1/3} + \left(\frac{v}{v_p} \right)^{1/3} \right] \quad (2)$$

where v_p and v are the volumes of particle B and the drop, respectively. The solubilization rate then becomes

$$k_{cp} = \beta_p q_p N_{\text{drop}} N_p \quad (3)$$

where β_p is the coalescence efficiency in drop-reactant particle collisions, and N_p is the number density of reactant B particles.

2.3.3. Reaction inside a Drop (k_r) (Figure 2c). Relevant reaction rates reported in literature have been used for the hydrolysis of hydride and the carbonation of lime. The reaction rate in the former case is zero order,³⁷ whereas in the case of the latter it is first order with respect to the hydroxyl ion concentration.^{26,38}

2.3.4. Coalescence-Exchange between Drops (k_c) (Figure 2d). From eq 2, the Brownian collision frequency of two equal-sized drops reduces to

$$q_d = \frac{8k_B T}{3\mu} \quad (4)$$

If the drop population number densities are n_1 and n_2 , then the coalescence-exchange rate is given by

$$k_c = \beta_d q_d n_1 n_2 \quad (5)$$

where β_d is the coalescence efficiency in drop–drop collisions. As shown in Figure 2d, coalescence of two drops results in exchange of dissolved molecules and redispersion of the dimer back into two equal-sized drops. From eq 5, we calculate the combined rate of coalescence-exchange, assuming that the exchange and redispersion rates are very fast. Typically, a dimer lifetime is about 25 μ s,³⁹ whereas the coalescence time scale is of the order of 0.1 s (Table 1). Hence, redispersion can be treated as instantaneous.

2.3.5. Nucleation of a Solid Particle C(s) in a Drop (k_n) (Figure 2e). The nucleation rate of liquid-phase product molecules [C(l)] to form a nucleus of solid particle [C(s)] in a drop is calculated from the classical nucleation theory of homogeneous nucleation. As quoted by Adamson⁴⁰ and discussed in Bandyopadhyaya et al.,^{25,26} this is given as

$$k_n(i, t) = 0 \quad \text{for } i < n^* \\ = iA \exp\left(\frac{-16\pi\sigma^3 v_m^2}{3(k_B T)^3 [\ln(\lambda(t))]^2}\right) \quad \text{for } i \geq n^* \quad (6)$$

TABLE 1: Time-Scale Estimates from Experiments

event	expression	time scale (s)	
		hydrolysis of hydride ¹⁴	carbonation of lime ¹³
transport of reactant A to drops (τ_m)	$1/k_m$	10	10
solubilization of reactant B in drops (τ_{cp})	$1/\beta_p q_p N_p$	10^{-1}	10
reaction (τ_r)	$1/k_r$	10^{-19}	10^{-5}
coalescence-exchange of drops (τ_c)	$1/\beta_d q_d N_{drop}$	10^{-1}	10^{-1}
coalescence of nonnucleated and nucleated drops (τ_{cn})	$1/\beta_d q_d N_1$	1	1
nucleation (τ_n)	$1/k_n(n^*)$	10^{-10}	10^{-1}
growth (τ_g)	v_{drop}/q	10^{-11}	10^{-10}

TABLE 2: Conclusions from Time-Scale Analysis^a

time-scale comparison	conclusion
(i) $\tau_c \gg \tau_r$ $\tau_{cn} \gg \tau_r$ $\tau_m > \tau_{cp} \gg \tau_r$ (only for HH) $\tau_m \approx \tau_{cp} \gg \tau_r$ (only for CL)	instantaneous reaction of A and B reactant A addition is rate-controlling
(ii) $\tau_g < \tau_n$	instantaneous growth of C(s) particle either none or one particle in a drop
(iii) $\tau_c < \tau_m$ $\tau_c < \tau_{cn}$	
$\tau_c \leq \tau_n$ (only for CL)	{ coalescence-exchange faster than nucleation Poisson distribution of C(l) molecules in nonnucleated drops PBE required only for nucleated drops
$\tau_c \gg \tau_n$ (only for HH)	{ coalescence-exchange slower than nucleation inapplicability of Poisson distribution for nonnucleated drops PBE for both nucleated and nonnucleated drops

^a Applicable to both HH and CL experiments, except when indicated otherwise. HH = hydrolysis of hydride;¹⁴ CL = carbonation of lime.¹³

where σ is the interfacial tension between solid nuclei and surrounding drop liquid, v_m is the volume of one C(s) molecule, λ is the supersaturation ratio of C(l), and n^* is the critical number of C molecules in a nucleus. Isolated drops in a w/o microemulsion solution have a distribution in the number of solute molecules, which change with time. There are no concentration gradients inside a particular drop because of its very small size. So eq 6 is used to calculate the nucleation rate in each drop, as a function of its changing supersaturation.

Although we have used homogeneous nucleation theory, the possibility of heterogeneous nucleation exists. The microenvironment in the interior of a drop is complex because it contains surfactant headgroups, counterions, reactant molecules, and bound and free water. These species may induce or prevent nucleation through various interaction forces. Preliminary molecular dynamics (MD) studies^{41,42} have been performed very recently to account for some of these interactions, but no general nucleation rate expression or trends have emerged.

2.3.6. Growth of Solid Particle C(s) in a Drop (k_g) (Figure 2f). The growth rate of a solid product particle [C(s)] in a drop is estimated by applying eq 2 between a C(l) molecule and C(s) present within the drop.

2.4. Conclusions from Time Scales. From Tables 1 and 2, for both hydrolysis of hydride and carbonation of lime, the reaction rate is very fast compared to coalescence-exchange of drops because $\tau_c \gg \tau_r$ and $\tau_{cn} \gg \tau_r$. For the hydrolysis of hydride, in addition, $\tau_m > \tau_{cp} \gg \tau_r$, implying that the rate of transport of A molecules into drops is slower than the rate of solubilization of particle B and the reaction rate is instantaneous

compared to these. Therefore, any molecule of reactant A entering a drop reacts very fast. So the overall product formation rate depends on the rate of transport of A (Table 2). For carbonation of lime, $\tau_m \approx \tau_{cp} \gg \tau_r$, meaning that the rates of transport of A and solubilization of B are comparable and the rate of reaction is faster than both of these. Nevertheless, it is known that initially each drop contains about 25 molecules of B, and once gas flow is started both A and B come to drops at equal rates. So each drop on an average would have a greater number of B molecules than A. Therefore, it can be concluded that the overall rate of formation of product is controlled by the rate of transport of reactant A.

When a nonnucleated drop develops supersaturation with respect to C(l), either a single nucleus can form and grow to exhaust the supersaturation or many nuclei can form simultaneously. Similarly, when nucleated and nonnucleated drops coalesce, the particle in the former can consume the supersaturation generated (in the dimer) or a new nucleus can form. The latter outcome can again lead to multiple C(s) particles in a single drop. Therefore, the relative rates of nucleation and growth of individual particles in a drop will determine whether the drop will have one or multiple particles. Our time-scale estimates show that τ_n is one (hydrolysis of hydride) or several (carbonation of lime) orders of magnitude higher than τ_g , implying that nucleation is slower than growth. So a nucleated drop can have only a single particle in it and the rest of the supersaturation is consumed instantaneously by growth of this single particle. This obviates the need to write separate PBE for particle population in each drop.

A drop having C(l) is affected by three events: (i) C(l) molecules formed by reaction, (ii) C(l) molecules lost or gained due to coalescence with other drops, and (iii) C(l) molecules lost due to nucleation. The relative rates of these three events will determine the distribution of C(l) in the population of nonnucleated drops. From Table 1, for both cases, $\tau_c < \tau_m$ and $\tau_c < \tau_{cn}$, which implies that before new C(l) molecules are added to a nonnucleated drop either by transport of reactant and reaction or by coalescence with other drops, the nonnucleated drops coalesce much faster among themselves and exchange their contents. In addition, for carbonation of lime, $\tau_c \leq \tau_n$, so the rate of coalescence between drops is faster than nucleation. In this limit, the distribution of the number of molecules of C(l) in nonnucleated drops attains an equilibrium Poisson distribution. This therefore obviates the need to write PBE for nonnucleated drops in this special case.²⁶ However, for hydrolysis of hydride, $\tau_c \gg \tau_n$, so nucleation occurs much faster than coalescence-exchange between drops. Because of faster nucleation, changes in the mean number of C(l) molecules in the nonnucleated drop population is faster than the rate at which drop coalescence-exchange can redistribute the C(l) molecules over this whole population. So an equilibrium Poisson distribution is not established, unlike the previous case. Therefore, in general, we have to account for such rapid changes in the state

of the nonnucleated drops by explicitly writing a PBE for this particular population. So we conclude that reaction and growth can be treated as instantaneous; transport of reactant A, coalescence-exchange of drops, and nucleation are slower and rate-controlling steps. Time-scale-based conclusions are summarized in Table 2.

The time scales reported in Table 1 are calculated from the experimental data available at time $t = 0$. Of all of the elementary processes (Figure 2), reactant A addition (as gas or liquid) and nucleation of C are unimolecular processes, whereas others are bimolecular. However, out of these, rates of reactant A addition, solubilization of reactant B, coalescence-exchange of microemulsion drops, and growth of nanoparticles are constant in time. In contrast, only reaction and nucleation rates depend on the number of molecules in a drop, which change with time.

The reaction time scale is very small (about 6 orders less) and hence instantaneous, compared to either transport of reactant A or solubilization of reactant B. So any change in the reaction time scale during the process will not affect the conclusions of time-scale analysis. As far as nucleation is concerned, only drops having sufficient number of C(l) molecules ($\geq n^*$) can nucleate. However, because of the low value of the mean number of C(l) molecules per drop, the number density of drops having n^* molecules or more is substantially low. Furthermore, among these drops that can potentially nucleate, most of the drops will have n^* molecules, implying that this group will have the highest nucleation rate. Therefore, we make a conservative estimate and calculate the nucleation rate corresponding to drops having n^* number of C(l) molecules. Because our models include rate expressions of nucleation, any variation in this during the process is automatically accounted for. To summarize, time-scale conclusions estimated from initial conditions are valid throughout the process.

3. Population Balance Model

It is sufficient to track only the product molecules in both forms [C(l) and C(s)] and to neglect the distribution of reactant molecules in the drops. So the drops can be classified as nonnucleated and nucleated depending upon whether they have C(l) or C(s), respectively. The nondimensional number densities with respect to the initial number of drops are defined as follows

$$\bar{n}_0(i,t) = \frac{n_0(i,t)}{N_{\text{drop}}} \quad \text{for } i = 0, 1, 2 \dots \infty \quad (7)$$

$$\bar{n}_1(i,t) = \frac{n_1(i,t)}{N_{\text{drop}}} \quad \text{for } i = n^*, (n^* + 1), (n^* + 2) \dots \infty$$

3.1. PBE for Nonnucleated Drops. The rate of change of number density of the subclass $\bar{n}_0(i,t)$ is given by the following PBE.

$$\begin{aligned} \frac{d\bar{n}_0(i,t)}{dt} &= k_m \bar{n}_0(i-1,t) - k_m \bar{n}_0(i,t) - \beta_d q_d N_{\text{drop}} \bar{n}_0(i,t) + \\ &\frac{\beta_d q_d N_{\text{drop}}}{2} \sum_{j=0}^{\infty} \sum_{k=0}^{\infty} \bar{n}_0(j,t) \bar{n}_0(k,t) E(i, j+k) - k_n(i,t) \bar{n}_0(i,t) \end{aligned} \quad \text{for } i = 1, 2, 3 \dots \infty \quad (8)$$

The first two terms on the right-hand side are generation and loss of $\bar{n}_0(i,t)$ due to transport of reactant molecules into the

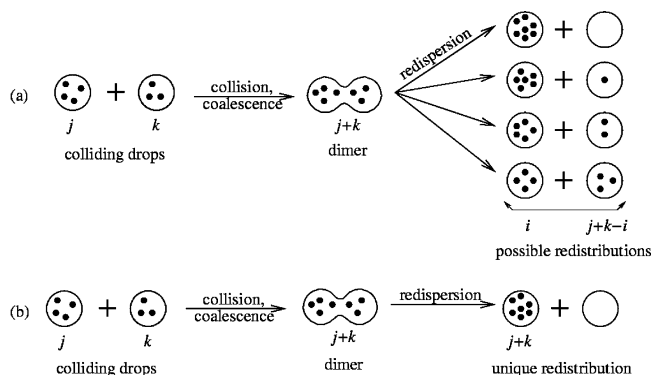


Figure 3. (a) Binomial and (b) cooperative redistribution of molecules.

drop. The third term accounts for loss due to coalescence with any other drop in the population. The fourth term is for generation due to coalescence-exchange between two appropriate nonnucleated drops. The last term in eq 8 is the loss term due to nucleation of C(l) into solid C(s).

Elaboration of the fourth term is possible from Figure 3, which shows binomial and cooperative redistribution mechanisms. In the case of the binomial (Figure 3a), two drops having j and k molecules in number, respectively, coalesce to form a dimer. When the dimer redisperses, $(j+k)$ molecules are randomly distributed between the two new drops. Each outcome is associated with a probability function $E(i, j+k)$. In contrast, cooperative redistribution (Figure 3b) results in a transfer of all of the molecules of the dimer into one of the two new daughter drops and the other one becomes empty.

The kinetics of solubilize exchange due to collision-coalescence of drops in both water-in-oil and oil-in-water microemulsions have been well established using fluorescence quenching and triplet energy transfer techniques, and a wide range of redistribution models were proposed. The fluorescence decay experiments of Atik and Thomas^{43,44} consistently showed that the exchange of molecules during coalescence of drops followed binomial redistribution. Furthermore, binomial redistribution mechanism leads to Poisson distribution of the number of molecules in a drop, when the drop population attains equilibrium. The kinetics of fluorescence decay derived from this Poisson distribution showed excellent comparison with their experiments, confirming the original binomial redistribution mode. Independently, Bommarius et al.⁴⁵ also implemented binomial redistribution in PBE to estimate the coalescence-exchange rate constant from their experiments. Their estimated rate constant matched very well with others.⁴⁶ Therefore, in the present PBE model of nanoparticle formation, binomial redistribution has been used. So the fourth term $E(i, j+k)$ in eq 8 is the expectation value for a drop to get i molecules on redispersion from a total of $(j+k)$ molecules in the dimer. Because nonnucleated drops are indistinguishable, the expression for $E(i, j+k)$ is given by binomial probability as follows.

$$E(i, j+k) = \frac{2(j+k)!}{i!(j+k-i)!} \left(\frac{1}{2}\right)^{(j+k)} \quad (9)$$

Various other modes of redistribution had been used first by Hatton et al.⁴⁷ in formulating their PBEs, for modeling solute exchange between drops. However, other than binomial, they are neither experimentally supported nor do the authors address nanoparticle formation in their work.

3.2. PBE for Nucleated Drops. The rate of change of number density of the subclass $\bar{n}_1(i,t)$ is given by the following PBE.

$$\frac{d\bar{n}_1(i,t)}{dt} = k_m \bar{n}_1(i-1,t) - k_m \bar{n}_1(i,t) - \beta_d q_d N_{\text{drop}} \bar{n}_1(i,t) \sum_{j=1}^{\infty} \bar{n}_0(j,t) + \beta_d q_d N_{\text{drop}} \sum_{j=1}^{i-n^*} \bar{n}_1(i-j,t) \bar{n}_0(j,t) + k_n(i,t) \bar{n}_0(i,t) \quad \text{for } i = n^*, (n^*+1), (n^*+2) \dots \infty \quad (10)$$

Except for the fourth term on the right-hand side, the other terms in eq 10 have the same meaning as those in eq 8. The fourth term accounts for growth of C(s) in a nucleated drop, while it coalesces with other nonnucleated drops.

The nondimensional number density of empty drops, $\bar{n}_0(0,t)$, can be obtained using the normalization condition

$$\bar{n}_0(0,t) + \sum_{i=1}^{\infty} \bar{n}_0(i,t) + \sum_{i=n^*}^{\infty} \bar{n}_1(i,t) = 1 \quad (11)$$

3.3. Moment Equations. Instead of solving individual number densities of nucleated drops from eq 10, it is sufficient to solve for moments of $\bar{n}_1(i,t)$ population for comparison with experimental measurements of mean size and coefficient of variance of particle size. The n th moment of nondimensional number density functions are defined as

$$M_0^{(n)}(t) = \sum_{i=0}^{\infty} i^n \bar{n}_0(i,t) \quad (12)$$

$$M_1^{(n)}(t) = \sum_{i=n^*}^{\infty} i^n \bar{n}_1(i,t)$$

From eqs 10 and 12, we get moment equations for nucleated drops:

$$\frac{dM_1^{(0)}(t)}{dt} = \sum_{i=n^*}^{\infty} k_n(i,t) \bar{n}_0(i,t) \quad (13)$$

$$\frac{dM_1^{(1)}(t)}{dt} = k_m M_1^{(0)}(t) + \beta_d q_d N_{\text{drop}} M_0^{(1)}(t) M_1^{(0)}(t) + \sum_{i=n^*}^{\infty} i k_n(i,t) \bar{n}_0(i,t) \quad (14)$$

$$\frac{dM_1^{(2)}(t)}{dt} = k_m [M_1^{(0)}(t) + 2M_1^{(1)}(t)] + \beta_d q_d N_{\text{drop}} [M_0^{(2)}(t) M_1^{(0)}(t) + 2M_0^{(1)}(t) M_1^{(1)}(t)] + \sum_{i=n^*}^{\infty} i^2 k_n(i,t) \bar{n}_0(i,t) \quad (15)$$

$\bar{n}_0(i,t)$, $M_0^{(1)}$, and $M_0^{(2)}$ in eqs 13–15 are calculated from eqs 8 and 12. The set of coupled first-order ordinary differential eqs 8 and 13 to 15 are solved numerically by the Runge–Kutta method⁴⁸ using the following initial conditions.

$$\bar{n}_0(0,t=0) = 1 \quad (16)$$

$$\bar{n}_0(i,t=0) = 0 \quad \text{for all } i = 1, 2, 3, \dots$$

$$M_1^{(0)}(t=0) = 0$$

$$M_1^{(1)}(t=0) = 0$$

$$M_1^{(2)}(t=0) = 0$$

The sensitivity of the numerical results was checked, and inclusion of terms beyond $i = 20$ in the equations gave no further variation in results. The mean diameter and coefficient of variation of nanoparticle diameter are obtained by the following formulas.

$$d_p(t) = \left[\frac{6M_p}{\pi \rho N_A} \frac{M_1^{(1)}(t)}{M_1^{(0)}(t)} \right]^{1/3} \quad (17)$$

$$CV(t) = \frac{\sqrt{\left(\frac{M_1^{(2)}(t)}{M_1^{(0)}(t)} \right)^{1/3} - \left(\frac{M_1^{(1)}(t)}{M_1^{(0)}(t)} \right)^{2/3}}}{\left(\frac{M_1^{(1)}(t)}{M_1^{(0)}(t)} \right)^{1/3}} \quad (18)$$

4. Monte Carlo Simulation Scheme

MC simulation of dynamic processes can be handled using the concept of the interval of quiescence (IQ) proposed by Shah et al.³⁰ The scheme used in the present work is an extension of the IQ-based simulation of Bandyopadhyaya et al.²⁹ In addition to accounting for nucleation and coalescence-exchange, in the present simulation we include transport of reactant through oil medium and solubilization of reactant particle inside drops.

The simulated system starts with a total of N drops of appropriate type and size. For lime carbonation, each drop is initialized with 25 $\text{Ca}(\text{OH})_2$ molecules (Section 2.2.), whereas for hydride hydrolysis, the drops have no reactant to start with. Reaction and growth of product particles occur instantaneously (Table 2). Therefore, the four remaining events, shown in Figure 2a, b, d, and e, are accounted for in the simulation. Selection of a particular event among these four is based on its relative frequency at a given instant of time. For a population of N drops, the total transport frequency of reactant A is $f_m = k_m N$; the total solubilization frequency of reactant B is $f_{cp} = \beta_p q_p N_p N$; the total frequency of coalescence-exchange between drops is $f_c = (1/2) \beta_d q_d N_{\text{drop}} N$, and the total nucleation frequency is $f_n(t) = \sum_{j=1}^N k_{n,j}(l,t)$. Here $k_{n,j}(l,t)$ is the nucleation rate in the j th drop having l number of C(l) molecules.

The probability of the occurrence of an i th event is

$$p_i(t) = \frac{f_i}{f_t(t)} \quad (19)$$

where

$$f_t(t) = f_m + f_{cp} + f_c + f_n(t)$$

IQ, the time interval between successive events is then given by

$$\tau_Q(t) = - \frac{\ln(1-R)}{f_t(t)} \quad (20)$$

Starting from time $t = 0$, once the simulation clock is advanced by the time interval τ_Q , then a particular event is selected according to the conditions given below (Figure 4).

At any particular MC step, if

(i) $0 \leq R < p_m$ then a drop is randomly selected and one A molecule is added.

(ii) $p_m \leq R < (p_m + p_{cp})$ then a drop is randomly selected and one B molecule is added.

(iii) $(p_m + p_{cp}) \leq R < (p_m + p_{cp} + p_c)$ then any two drops are randomly selected. If they have reactant A and B, respec-

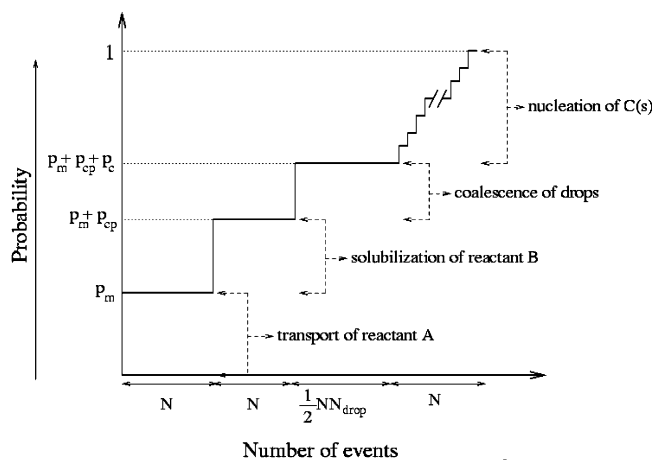


Figure 4. Selection of events in MC simulation using random numbers.

tively, then product molecules C(l) form instantaneously and excess reactant molecules are binomially redistributed over the two daughter drops. If one of the colliding drops has a particle, then the entire C(l) formed leads to particle growth and excess reactant is binomially redistributed. Instead, if both the drops have particles, then C(l) and excess reactants are binomially redistributed and each particle grows.²⁹

(iv) $(p_m + p_{cp} + p_c) \leq R < 1$, because of the nonuniform distribution of C(l) in the drops, their nucleation rates are different and are also a function of time. The i th drop can nucleate if it satisfies the following criterion.

$$\left(p_m + p_{cp} + p_c + \frac{\sum_{j=1}^{i-1} k_{n_j}(l,t)}{\sum_{j=1}^N k_{n_j}(l,t)} \right) \leq R_1 < \left(p_m + p_{cp} + p_c + \frac{\sum_{j=1}^i k_{n_j}(l,t)}{\sum_{j=1}^N k_{n_j}(l,t)} \right)$$

5. Results and Discussion

Various parameters and constants used in the model and simulation are listed in Table 3.

5.1. Hydrolysis of Hydride.¹⁴ *5.1.1. Comparison with Experiments.* Delfort et al.¹⁴ have reported only the final nanoparticle size and shape (cylindrical disk) at the end of 5 h. Our model does not address the issue of particle shape because we assume isotropic growth, leading to a spherical particle. So we compare the model results with the volume equivalent diameter of a sphere, the volume being calculated from the experimentally reported mean diameter and thickness of the disk.

Predictions from the PBE model and MC simulation with binomial redistribution compare very well with the experimental particle size at 5 h and are shown in Figure 5a. The close match of experiment with both the MC simulation and the PBE model justify the assumptions and simplifications (based on time-scale analysis) adopted in writing the PBEs. In the stochastic MC simulation, each random elementary event is executed sequentially, one at a time. In the deterministic PBE model, in contrast, the average rates of these events are used and the process is represented by a set of ordinary differential equations. The excellent agreement between the two implies that the formula-

TABLE 3: Parameters Used in the PBE Model and MC Simulation

parameter	hydrolysis of hydride ¹⁴	reference	carbonation of lime ^{13,a}
A	$6.5 \times 10^{11} \text{ s}^{-1}$	59	278.1 s^{-1}
d_{drop}	$2.2 \times 10^{-9} \text{ m}$	35	$2.44 \times 10^{-9} \text{ m}$
k_m	0.0438 s^{-1}	14	0.112 s^{-1}
K_s	$3.35 \times 10^{-6} \text{ mol}^2 \text{ lit}^{-2}$	b	$3.31 \times 10^{-12} \text{ mol}^2 \text{ lit}^{-2}$
N	20 000	c	20 000
N_{agg}	95	35	27
N_{drop}	$1.038 \times 10^{24} \text{ m}^{-3}$	14	$4.31 \times 10^{24} \text{ m}^{-3}$
N_p	$1.092 \times 10^{17} \text{ m}^{-3}$	14	$9.24 \times 10^{16} \text{ m}^{-3}$
n^*	5	26	5
Q	$2.494 \times 10^{-6} \text{ kg s}^{-1}$	14	$7.934 \times 10^{-6} \text{ kg s}^{-1}$
T	283 K	14	298 K
v_{drop}	$5.572 \times 10^{-27} \text{ m}^3$	35	$4.68 \times 10^{-27} \text{ m}^3$
v_m	$5.485 \times 10^{-29} \text{ m}^3$	calculated	$6.13 \times 10^{-29} \text{ m}^3$
v_{me}	$5.523 \times 10^{-4} \text{ m}^3$	14	$2.251 \times 10^{-4} \text{ m}^3$
v_p	$5.235 \times 10^{-19} \text{ m}^3$	calculated ^d	$5.235 \times 10^{-19} \text{ m}^3$
α	0.6	14	1.0
β_d	1×10^{-6}	fitted ^e	7×10^{-6}
β_p	0.055	26	0.055
μ	$0.001 \text{ kgm}^{-1}\text{s}^{-1}$	standard value	$0.05 \text{ kgm}^{-1}\text{s}^{-1}$
σ	0.065 Nm^{-1}	59	0.097 Nm^{-1}

^a All parameters for this experiment are taken from ref 26. ^b Solubility of Ca(OH)₂ in the methanol–water mixture is calculated based on the proportionality of the solubility product with the cube of the dielectric constant. ^c Simulations with N up to 100 000 gave the same results. ^d Using a Ca(OH)₂ particle diameter of 1 micrometer. ^e Order of magnitude similar to ref 26.

tion of PBE based on average rates is sufficient to describe the process of nanoparticle formation.

However, MC simulation with cooperative redistribution underpredicts the experimental particle size. This is expected because a large number of product molecules accumulates in a single drop and increases the nucleation rate in this exchange mode. This yields more nuclei and smaller-sized particles for the same total amount of product. In contrast, in binomial redistribution mode, the reactant and product molecules are redistributed over both of the daughter drops, in nearly every coalescence, making more molecules available for growth and suppressing nucleation. As discussed in Section 3, binomial redistribution is the correct mode and hence provides a very good comparison with experiments. Recently, Kumar et al.⁴⁹ modeled nanoparticle formation on mixing two microemulsion solutions (containing different presolubilized reactants), featuring correct consideration of several classes of population. However, they used cooperative redistribution in their PBE; thus, their predicted particle size was also smaller compared to experiments.

The coefficients of variation (CV) of nanoparticle diameter from the model and simulation are shown in Figure 5b. Although experimental CVs are unavailable, it can be seen that the model predicts moderately monodisperse ($CV = 0.18$) particle size. This is due to the very high nucleation rate, leading to the formation of a large number of nuclei very early in the process. Later these nuclei grow more or less equally. As expected, MC simulation with cooperative redistribution predicts a slightly higher CV than binomial redistribution in the beginning, whereas simulation with binomial redistribution matches very well with the PBE results throughout. This once again confirms the ability to address nanoparticle formation by both PBE and simulation so that not only mean size but also higher order statistic can be predicted successfully.

5.1.2. Effect of Drop Size. Experimentally, drop diameter can be varied easily by changing the microemulsion composition, thereby controlling the size of the nanoparticles. Figure 5c shows that on varying the drop diameter from 1 to 7 nm, there is no

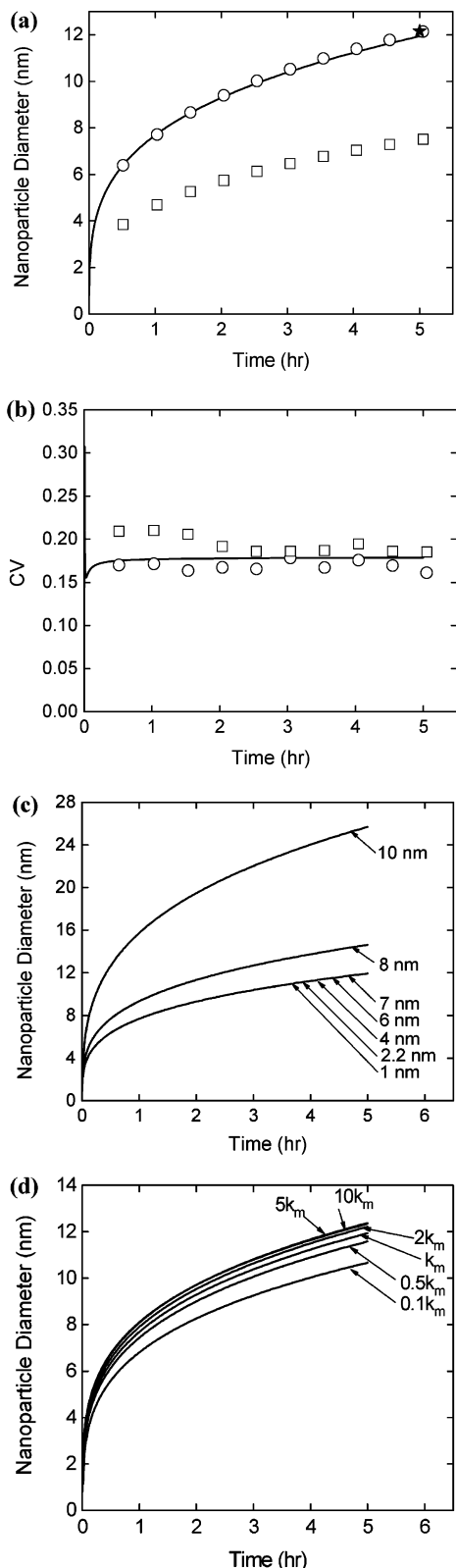


Figure 5. Temporal evolution of $\text{Ca}(\text{OH})_2$ nanoparticle: (a) mean diameter; (b) coefficient of variation (CV). (★) Experimental;¹⁴ (—) PBE model with binomial redistribution; (○) MC simulation with binomial redistribution; (□) MC simulation with cooperative redistribution. (c) Effect of drop size and (d) effect of water addition rate on mean nanoparticle diameter (parameter values shown against each curve in c and d).

influence on nanoparticle size, as predicted by the PBE model. However, beyond this, further increase in drop diameter results in a significant increase in particle size. The curve labeled 2.2

nm corresponds to a reported experimental drop size.¹⁴ In general, an increase in drop size and therefore volume, keeping the total amount of product $\text{C}(\text{l})$ constant, reduces supersaturation in a single drop. This leads to a lower nucleation rate and therefore a lower number of particles with increased mean size. These arguments are valid in the present case for drop diameters beyond 7 nm. However, for drop diameters from 1 to 7 nm, we find, $k_n(n^*) \gg k_m$ and $k_n(n^*) \gg k_c$ so that nucleation rate is almost instantaneous compared to mass transport or coalescence-exchange. Therefore, particle nucleation in this range of drop diameter is virtually unaffected, translating to no change in particle number and size. However, beyond 7 nm, $k_n(n^*) \leq k_m$ and $k_n(n^*) \leq k_c$ so that nucleation becomes dependent on how fast water is added and supersaturation builds up by reaction and drop-drop coalescence. This results in the expected increase in particle size as shown in Figure 5c.

We also know (as shown in eq 5 and Table 1) that rate constants are inversely related to time constants. So the above discussion and conclusion extends naturally to time-scale comparison as well.

5.1.3. Effect of Water Addition Rate. Figure 5d shows the effect of increasing water addition rate on $\text{Ca}(\text{OH})_2$ nanoparticle size. The curve labeled k_m corresponds to the experimentally reported water addition rate.¹⁴ As we change it from $0.1 k_m$ to $10 k_m$, the model predicts a small increase in particle size at lower k_m values, but does not show further increase at higher k_m . In all cases, there is excess CaH_2 reactant present in the system to ensure that water addition will be the rate-limiting step. This implies that with increase in k_m , we have a proportional increase in the total amount of $\text{Ca}(\text{OH})_2$ formed in the system. As more $\text{Ca}(\text{OH})_2$ (l) molecules form in drops with increased rate of water addition, it can lead to either increased nucleation or particle growth by coalescence-exchange. The marginal increase in mean particle size on going from $0.1 k_m$ to k_m implies that nucleation is more favored over growth. While on going from k_m to $10 k_m$, the mean particle size remains virtually unaffected, resulting in a proportional increase in the number of particles at such high supersaturation, rather than any additional growth. Therefore, the production rates of nanoparticles can be increased significantly by increasing the water addition rate, without much variation of particle size, taking advantage of the dominance of nucleation in this system.

However, some other relevant variables, for example, nature of oil, surfactant, its counterion, cosurfactant, viscosity of oil, and so forth do not affect mean particle size and size distribution significantly. Independence of particle size on the nature of the cosurfactant has been shown recently.¹⁸

5.2. Carbonation of Lime.¹³ Figure 6a and b shows a comparison of the results of the lime carbonation experiment¹³ with both the PBE model and MC simulation. Figure 6a shows an excellent match of the evolution of the mean diameter of CaCO_3 nanoparticles with time when binomial redistribution is used. Previously, Bandyopadhyaya et al.²⁶ had also predicted this experimental data from their PBE model with equal success. They did not explicitly include the redistribution mechanism in their PBE. However, their assumption of the Poisson distribution of $\text{C}(\text{l})$ in nonnucleated drops implied that the coalescence-exchange process was by binomial redistribution and occurred quite frequently so that equilibrium Poisson distribution could be assumed. Hence, their model becomes a limiting case of the present model, when coalescence-exchange is faster than nucleation. As explained previously, cooperative distribution gives smaller particle size (Figure 6a).

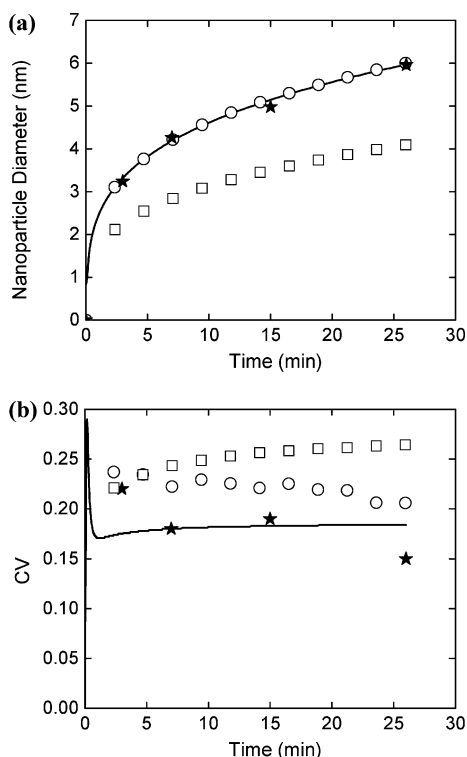


Figure 6. Temporal evolution of CaCO₃ nanoparticle: (a) mean diameter; (b) coefficient of variation (CV). (★) Experimental;¹³ (—) PBE model with binomial redistribution; (○) MC simulation with binomial redistribution; (□) MC Simulation with cooperative redistribution.

Coefficient of variation (*CV*) of particle size with time in Figure 6b compares well with experiments only toward the end of the process for both PBE and MC with binomial redistribution. The PBE model prediction of *CV* starts from zero (no particle to begin with) and has a very rapid rise at short times (not visible in the scale of Figure 6b) up to about 0.28. This is due to rapid nucleation resulting in particles of different size. *CV* then falls within about 1 min of process time down to 0.17, as nucleation slows down and stops, allowing all particles formed to grow by more or less equal extent. Unfortunately, there is no experimental data before 3 min to verify these predictions. Afterward there is a very small increase in *CV* between 1 and 5 min of process time, before it approaches a constant value of about 0.18, which is close to the experimental data points (Figure 6b). Thus, for most of the process the *CV* curve predicted by the PBE model falls within the range of experimental *CV* values and constitutes a reasonable agreement, although not exact.

The results of the MC simulation with the unrealistic cooperative redistribution diverge from experiments. This is because of higher variation in the growth process with the latter mode. It results in increased dispersity in particle size and, in turn, *CV* as well. In binomial redistribution, however, a smaller number of nuclei is formed, and the particles have more product molecules for growth, making them more equally available to all nuclei. This leads to a narrower distribution of particle size and, hence, a smaller *CV*.

The class of experiments involving hydrolysis of hydride is important to analyze because it operates in a regime where the nucleation rate far exceeds the rate of coalescence-exchange of drops, a domain in which none of the previously developed models apply. Data from this experiment,¹⁴ although limited in range, is therefore a good test for the models developed in the present work because the latter is applicable for arbitrary relative

rates of coalescence-exchange and nucleation. In addition, our results show the evolution of mean particle size and its variance for an opposite class of experiments, namely carbonation of lime, wherein the nucleation rate is much less. Thus, we have shown (from different experimental data) that both our PBE model and MC simulations are in general enough to incorporate widely divergent experimental conditions, and thereby successfully predict temporal evolution in mean size and variance of nanoparticle size distribution.

5.3. Deterministic and Stochastic Methods. The particle formation mechanism has been addressed in this paper by two formalisms: deterministic PBE and stochastic simulation. The former regards time evolution of the system at hand (having coupled mass transport, collision, and nucleation) to be continuous and deterministic, and hence models it by a set of coupled differential equations, as in PBEs. Although in many cases this is true, in reality the evolution is not continuous because molecular population in a drop changes by a discrete integer amount. Furthermore, collisions in a system of thermally equilibrated molecules or nucleation in a supersaturated medium occur randomly so that we should refer to collision and nucleation probabilities per unit time, rather than collision or nucleation rates. Fundamentally, the system is therefore neither continuous nor deterministic.

In the alternative route pursuing the stochastic approach, the state of the system can be described by a master probability density function in continuous state variables, like particle size, concentration, and so forth. This leads to a hierarchy of product density equations of different order, giving both the mean quantities and fluctuations about the mean.⁵⁰ Similar stochastic formulation in chemical kinetics⁵¹ or its adaptation⁵² has resulted in other forms of master equations using discrete state variables, like number of molecules or discrete particle size. Although rigorous, these equations are often mathematically intractable, or unclosed in nature so that we have presently employed the stochastic MC simulation algorithm (derived from same stochastic arguments) for obtaining numerical results. In the simulation scheme, time evolution of the system is regarded to be discrete and the random events occur sequentially, one at a time, according to their relative frequency of occurrence. This therefore recognizes the inherent randomness of all of the elementary steps, namely, transport and solubilization of reactants, coalescence-exchange of drops and nucleation of particles, which is accounted by discrete changes in number and size of particles. Hence, our simulation follows the natural evolution of the process in time. In contrast, the time-averaged kinetic rates of random events over a large population are used for evolution in the PBE framework.

Hence, in some cases, the deterministic PBE will be unable to describe the inherent fluctuations and correlation in the molecular population levels, which the stochastic simulation algorithm can naturally account for.^{50,51} Although the deterministic PBE gives only mean number densities, the stochastic route in addition, provides fluctuations of all order about the mean. However, from our time-scale analysis, there can be at most only one nanoparticle in a single microemulsion drop. So, any fluctuation in the concentration of C(l) resulting from random nucleation in the microemulsion drop does not affect the nucleation or growth of any other particle in the system. Therefore, we are able to model by both deterministic and stochastic routes, giving very close results in particle characteristics for different experiments. Compared to this, Manjunath et al.^{50,53} showed that in the case of precipitation in a much bigger micrometer-sized emulsion drop, where more than one

particle could form in the drop, deterministic PBE and MC simulation results could be different. Thus, random nucleation in a small, confined particle population in an emulsion drop can cause large fluctuations in concentration and supersaturation, affecting further nucleation and particle growth in that drop. This results in fluctuations in the confined particle population characteristics as well, forcing PBE and MC results to differ. Extending the argument further, one can clearly see that if the particle population is large then a single collision, nucleation, or growth (by addition of discrete molecules) event does not make a substantial change in the particle number or size distribution, leading to concurrence of deterministic and stochastic description. This is indeed seen in bulk crystallization in a well-mixed system.⁵² A mathematical treatise on the connection between PBE and MC simulation can be found in Ramkrishna.⁵⁴

6. Conclusions

The mechanism of nanoparticle formation in water-in-oil microemulsion has been developed by systematically estimating time scales of various elementary steps. A deterministic PBE model and a stochastic MC simulation scheme have been proposed based on this mechanism, which further generalize and extend previous work.^{26,29} Both the model and simulation incorporate the mass transport of liquid or gaseous reactants from the continuous oil phase to water drops, solubilization of solid dispersed in oil, coalescence-exchange of water drops, and nucleation and growth of the nanoparticle. Molecular exchange of reactants and products after coalescence of drops is modeled by binomial redistribution of the contents of the dimer into daughter droplets. The proposed mechanism is validated under different controlling regimes, relevant to two broadly similar experiments: carbonation of lime¹³ and hydrolysis of hydride¹⁴ to give CaCO_3 and Ca(OH)_2 nanoparticles, respectively. Model and simulation predictions of temporal evolution of nanoparticle size and its coefficient of variation match very well with experiments. This proves that the PBE model developed in this paper is quite general and is applicable when both coalescence and nucleation rates are important or in the limits of one of them being rate-controlling. Furthermore, both a deterministic PBE model and a stochastic simulation scheme can account for the inherent randomness in the elementary events, providing complementary means to predict mean nanoparticle size and its variance. Also, we have clearly brought out the significance of implementing the correct binomial redistribution exchange mechanism on successful modeling of experimental data, in comparison to phenomenologically incorrect cooperative or other modes used earlier. The model and simulation provide size evolution data for time scales ranging from minutes (carbonation of lime) to many hours (hydrolysis of hydride), suggesting robustness of our calculation and credibility of the almost identical parameters used. Furthermore, we obtain temporal evolution of both the mean and standard deviation of nanoparticle size, supplementing experimental measurements in some cases.

Effect of easily controllable operational variables, for example, drop size and water addition rate, on mean Ca(OH)_2 particle size have been explored from the model. Below a drop diameter of 7 nm, nanoparticle size is not affected by an increase in size of the drop. This is possible because the nucleation rate is instantaneous compared to the water transport and coalescence-exchange rates, for drops in this size range. However, beyond a 7 nm drop size, the nucleation rate becomes comparable to other rates, thus showing an expected increase in size of

nanoparticle with that of the drop. However, when the addition rate of water (a reactant) to the microemulsion solution was independently varied both below and above the experimental rate of water addition, the model predictions show that the nanoparticle size would not change appreciably. This therefore implies that under certain general conditions nanoparticle synthesis can be scaled up for production by a simple increase of external reactant addition rate, without any undesirable change in particle size.

In general, inorganic nanoparticle formation via reactive precipitation has almost instantaneous reaction and particle growth rates in drops. This simplifies the population of drops into two types, nonnucleated and nucleated, both of which can be described by only one state variable, namely the number of product molecules in each drop or nanoparticle, respectively. However, when either reaction or growth is not instantaneous, additional classes of drops need to be identified with multiple state variables to account for more than one type of reactant and product molecules distinguishing the drops. Similar is the need when two microemulsion solutions are reacted. In this case, the mixing of reactants and the formation of a solid nanoparticle occur only via coalescence-exchange and not by external mass transport and solubilization. Our model can be suitably extended for these cases by writing multivariate PBEs for all classes of drops.

Both the model and simulation are very general and on making appropriate time-scale analysis can be modified to give further insight into the mechanism of nanoparticle formation in other colloidal self-assembled templates such as vesicles,⁵⁵ block copolymer micelles,⁵⁶ dendrimers,⁵⁷ and birefringent phases.⁵⁸ These templates are distinguished based on their confinement length scale and collision dynamics, features that our model can account for. Finally, in anisotropic nanoparticle synthesis, particles grow only in certain preferential directions because of different growth rates along different crystallographic axes. Our analysis can incorporate this effect if the finite growth rate data of particles along different crystal axes are available.

Glossary

A	Preexponential factor in the nucleation rate expression, s^{-1}
$C(l)$	C molecules in solubilized form
$C(s)$	C molecules in solid particle form
CV	Coefficient of variation of nanoparticle diameter
d_{drop}	Diameter of drop, m
d_p	Volume equivalent diameter of $C(s)$ particle, m
$E(i, j + k)$	Expectation value of having i molecules in a daughter droplet from a dimer containing $(j + k)$ molecules
f	Frequency of an individual event, s^{-1}
f_t	Total frequency of all events, s^{-1}
k	Rate constant, s^{-1}
k_B	Boltzmann constant, $1.3806 \times 10^{-23} \text{ J K}^{-1}$
K_s	Solubility product of C , $\text{mol}^2 \text{ lit}^{-2}$
$M^{(i)}$	i th moment of a population
M_p	Molecular weight of C , kg kmol^{-1}
M_w	Molecular weight of reactant A , kg kmol^{-1}
n^*	Critical number of molecules required for nucleation
$n(i)$	Number density of drops having i product molecules, m^{-3}
$\bar{n}(i)$	Nondimensional number density of drops having i product molecules
N	Total number of drops used in MC simulation
N_{agg}	Surfactant aggregation number

N_A	Avogadro's number, 6.023×10^{23} molecules/mole
N_{drop}	Total number density of drops, m^{-3}
N_p	Total number density of reactant B particles, m^{-3}
p	Probability of an event
Q	Mass flow rate of reactant A, kg s^{-1}
q_d	Brownian collision frequency of two drops, $\text{m}^3 \text{s}^{-1}$
q_p	Brownian collision frequency of a drop with a reactant B particle, $\text{m}^3 \text{s}^{-1}$
R, R_1	Uniformly distributed random variable in $[0, 1)$
T	Temperature, K
v_{me}	Total volume of microemulsion solution, m^3
v_{drop}	Volume of a single drop, m^3
v_m	Volume of one C(s) molecule, m^3
v_p	Volume of one reactant B particle, m^3

Greek Symbols

α	Fraction of reactant A transported into drops
β_d	Coalescence efficiency of drop-drop collision
β_p	Coalescence efficiency of drop-reactant particle collision
λ	Supersaturation ratio of C(l) (calculated as in ref 26)
μ	Viscosity, $\text{kg m}^{-1} \text{s}^{-1}$
ρ	Density of product, kg m^{-3}
σ	Interfacial tension between solid nuclei and surrounding drop liquid, N m^{-1}
τ	Time scale of an event, s
τ_Q	Interval of quiescence, s

Subscripts

0	Nonnucleated drop
1	Nucleated drop
c	Coalescence-exchange between nonnucleated drops
cn	Coalescence exchange of nucleated and nonnucleated drops
cp	Solubilization of reactant B into a drop
g	Growth of C(s)
m	Transport of reactant A
n	Nucleation of C(s)
r	Reaction of A and B

References and Notes

- Fendler, J. H. *Membrane Mimetic Chemistry*; John Wiley & Sons: New York, 1982.
- Pileni, M. P. *Langmuir* **1997**, *13*, 3266.
- Rees, G. D.; Evans-Gowing, R.; Hammond, S. J.; Robinson, B. H. *Langmuir* **1999**, *15*, 1993.
- Lisiecki, I. *J. Phys. Chem. B* **2005**, *109*, 12231.
- El-Sayed, M. A. *Acc. Chem. Res.* **2004**, *37*, 326.
- Alivisatos, A. P. *J. Phys. Chem.* **1996**, *100*, 13226.
- Eriksson, S.; Nylen, U.; Rojas, S.; Boutonnet, M. *Appl. Catal., A* **2004**, *265*, 207.
- Bakunin, V. N.; Suslov, A. Y.; Kuzmina, G. N.; Parenago, O. P. *J. Nanopart. Res.* **2004**, *6*, 273.
- Fendler, J. H. *Chem. Mater.* **2001**, *13*, 3196.
- Luisi, P. L. Concepts and pictographic models in reverse micelles. In *Kinetics and Catalysis in Microheterogeneous Systems*; Gratzel, M., Kalyanasundaram, K., Eds.; Marcel Dekker: New York, 1991; pp 115–134.
- Pileni, M. P. Structural changes of reverse micelles and microemulsions by adding solutes or proteins. In *Structure and Reactivity in Reverse Micelles*; Pileni, M. P., Ed.; Elsevier: Amsterdam, 1989; pp 44–53.
- Kandori, K.; Kon-No, K.; Kitahara, A. *J. Colloid Interface Sci.* **1988**, *122*, 78.
- Roman, J.-P.; Hoornaert, P.; Faure, D.; Biver, C.; Jacquet, F.; Martin, J.-M. *J. Colloid Interface Sci.* **1991**, *144*, 324.
- Delfort, B.; Born, M.; Chive, A.; Barre, L. *J. Colloid Interface Sci.* **1997**, *189*, 151.
- Delfort, B.; Normand, L.; Dascotte, P.; Barre, L. *J. Colloid Interface Sci.* **1998**, *207*, 218.
- Delfort, B.; Chive, A.; Barre, L. *J. Colloid Interface Sci.* **1997**, *186*, 300.
- Debuigne, F.; Jeunieu, L.; Wiame, M.; Nagy, J. B. *Langmuir* **2000**, *16*, 7605.
- Debuigne, F.; Cuisenaire, J.; Jeunieu, L.; Masereel, B.; Nagy, J. B. *J. Colloid Interface Sci.* **2001**, *243*, 90.
- Curri, M. L.; Agostiano, A.; Manna, L.; Monica, M. D.; Catalano, M.; Chiavarone, L.; Spagnolo, V.; Lugara, M. *J. Phys. Chem. B* **2000**, *104*, 8391.
- Ramkrishna, D. *Population Balances-Theory and Applications to Particulate Systems in Engineering*; Academic Press: San Diego, CA, 2001.
- Randolph, A. D.; Larson, M. A. *Theory of Particulate Processes-Analysis and Techniques of Continuous Crystallization*; Academic Press: San Diego, CA, 1988.
- Nagy, J. B. *Colloids Surf.* **1989**, *35*, 201.
- Hirai, T.; Sato, H.; Komazawa, I. *Ind. Eng. Chem. Res.* **1993**, *32*, 3014.
- Natarajan, U.; Handique, K.; Mehra, A.; Bellare, J. R.; Khilar, K. C. *Langmuir* **1996**, *12*, 2670.
- Bandyopadhyaya, R.; Kumar, R.; Gandhi, K. S.; Ramkrishna, D. *Langmuir* **1997**, *13*, 3610.
- Bandyopadhyaya, R.; Kumar, R.; Gandhi, K. S. *Langmuir* **2001**, *17*, 1015.
- Provis, J. L.; Vlachos, D. G. *J. Phys. Chem. B* **2006**, *110*, 3098.
- Van Hyning, D. L.; Klemperer, W. G.; Zukoski, C. F. *Langmuir* **2001**, *17*, 3128.
- Bandyopadhyaya, R.; Kumar, R.; Gandhi, K. S. *Langmuir* **2000**, *16*, 7139.
- Shah, B. D.; Ramkrishna, D.; Borwanker, J. D. *AIChE J* **1977**, *23*, 897.
- Voigt, A.; Adityawarman, D.; Sundmacher, K. *Nanotechnology* **2005**, *16*, s429.
- Jain, R.; Mehra, A. *Langmuir* **2004**, *20*, 6507.
- Ferrante, F.; Turco Liveri, V. *Colloids Surf., A* **2005**, *259*, 7.
- Singh, R.; Durairaj, M. R.; Kumar, S. *Langmuir* **2003**, *19*, 6317.
- Chive, A.; Delfort, B.; Born, Maurice.; Barre, L. *Langmuir* **1998**, *14*, 5355.
- Smoluchowski, M. V. *Phys. Z.* **1916**, *17*, 557.
- Kong, V. C. Y.; Foulkes, F. R.; Kirk, D. W.; Hinatsu, J. T. *Int. J. Hydrogen Energy* **1999**, *24*, 665.
- Danckwerts, P. V. *Gas-Liquid Reactions*; McGraw-Hill: New York, 1970; p 239.
- Fletcher, P. D. I.; Howe, A. M.; Robinson, B. H. *J. Chem. Soc., Faraday Trans. 1* **1987**, *83*, 985.
- Adamson, A. W.; Gast, A. P. *Physical Chemistry of Surfaces*; John Wiley & Sons: New York, 1997; p 331.
- Zahn, D. *Phys. Rev. Lett.* **2004**, *92*, 40801.
- Hamad, S.; Cristol, S.; Catlow, C. R. A. *J. Am. Chem. Soc.* **2005**, *127*, 2580.
- Atik, S. S.; Thomas, J. K. *J. Am. Chem. Soc.* **1981**, *103*, 3543.
- Atik, S. S.; Thomas, J. K. *Chem. Phys. Lett.* **1981**, *79*, 351.
- Bommarius, A. S.; Holzwarth, J. F.; Wang, D. I. C.; Hatton, T. A. *J. Phys. Chem.* **1990**, *94*, 7232.
- Zana, R.; Lang, J. Dynamics of microemulsions. In *Microemulsions: Structure and Dynamics*; Friberg, S. E., Bothorel, P., Eds.; CRC Press: Boca Raton, FL, 1988; pp 153–172.
- Hatton, T. A.; Bommarius, A. S.; Holzwarth, J. F. *Langmuir* **1993**, *9*, 1241.
- Gupta, S. K. *Numerical Methods for Engineers*; New Age International Ltd.: New Delhi, 1995.
- Kumar, A. R.; Hota, G.; Mehra, A.; Khilar, K. C. *AIChE J.* **2004**, *50*, 1556.
- Manjunath, S.; Gandhi, K. S.; Kumar, R.; Ramkrishna, D. *Chem. Eng. Sci.* **1994**, *49*, 1451.
- Gillespie, D. T. *J. Phys. Chem.* **1977**, *81*, 2340.
- Haseltine, E. L.; Patience, D. B.; Rawlings, J. B. *Chem. Eng. Sci.* **2005**, *60*, 2627.
- Manjunath, S.; Gandhi, K. S.; Kumar, R.; Ramkrishna, D. *Chem. Eng. Sci.* **1996**, *51*, 4423.
- Ramkrishna, D. *Chem. Eng. Sci.* **1981**, *36*, 1203.
- Meldrum, F. C.; Heywood, B. R.; Mann, S. *J. Colloid Interface Sci.* **1993**, *161*, 66.
- Selven, S. T.; Hayakawa, T.; Nogami, M.; Moller, M. *J. Phys. Chem. B* **1999**, *103*, 7441.
- Zhao, M.; Crooks, R. M. *Adv. Mater.* **1999**, *11*, 217.
- Tanori, J.; Pileni, M. P. *Langmuir* **1997**, *13*, 639.
- Klein D. K.; Smith M. D. *Talanta* **1968**, *15*, 229.